Experimental study of laminar flames obtained by the homogenization of three forest fuels

Towards characterization of the coupling between gas and solid phases in forest fires

VIRGINIE TIHAY[a], ALBERT SIMEONI[a], PAUL-ANTOINE SANTONI[a], JEAN-PIERRE GARO[b] AND JEAN-PIERRE VANTELON[b]

[a] SPE– UMR 6134 CNRS, University of Corsica, Campus Grossetti, BP 52, 20250 Corte, France Phone: (33) 495 450 121; Fax: (33) 495 450 162

[b] LCD – UPR 9028 CNRS, ENSMA, University of Poitiers, 1 avenue Clément Ader, Téléport 2 – BP 40109, 86961 Futuroscope Chasseneuil Cedex, France

Abstract – The aim of this work is to improve the understanding on the coupling between the gas and the solid phases occurring in forest fires. We studied three species representative of the Mediterranean vegetative cover (*Pinus pinaster*, *Erica arborea* and *Cistus monspeliensis*). We crushed them in order to decrease the geometrical effects and to focus on the heat and mass transfer occurring during their combustion. The coupling between the crushed fuels and the flame was studied experimentally from unsteady, axisymmetric, non-premixed, laminar flames. The thermal properties and the mass loss of the solid phase, the distribution of temperature in the two phases, the gases released by the fuels and the flame geometry were measured. The results showed that the thermal degradation of the solid phase depends on the thermal properties of the sample, on the ash content and on the surface-to-volume ratio. Although the mass burning rate of the samples mainly controls the flame dynamics, the degradation gases proved to influence its temperature and geometry.

Keywords: laminar flame; forest fuels, degradation gases, coupling between phases.

NOMENCLATURE

Heat flow	HF	W
Heating value per mass of air	Δh_a	$kJ.kg^{-1}$
Length	L	M
Mass	m	Kg
Reaction enthalpy	Δh	$kJ.kg^{-1}$
Specific heat capacity	C_p	$J.kg^{-1}.K^{-1}$
Stoechiometric coefficient in air	f_s	
Temperature	T	K
Volume	V	m^3
Thermal diffusivity ($\lambda/\rho Cp$)	a	$m^2.s^{-1}$
Width	l	M

Greek symbols

Bulk density	ρ_{bulk}	$kg.m^{-3}$
Fuel packing ratio	α	
Mass density	ρ	$kg.m^{-3}$
Surface-to-volume ratio	σ	m^{-1}
Thermal conductivity	λ	$W.m^{-1}.K^{-1}$

Subscripts

Empty pan	Empty
Ethanol	Ethanol
Mean value	Mean
Pan with reference sample	Reference
Pan with sample	Sample
Time increment	K

1 Introduction

Fires devastate regularly forests and scrublands as well as populated areas all over the world. Foresters and fire fighters are faced with problems such as the management of wildland/urban interfaces and safety zones. To deal with this kind of situations, the fire phenomenon and specially the combustion of vegetation need to be better understood. The mechanisms occurring in forest fires are strongly coupled and this aspect was poorly studied up to now. Although the experiments at field scale are valuable to validate the numerical models of fire spread, they are not appropriated to investigate the coupling between flames and combustible fuels. Experiments at laboratory scale allow focusing on accurate phenomena as the fire parameters are monitored and controlled more easily. Among the experiments conducted at laboratory scale to investigate the burning of vegetative fuels, the following kinds of studies are carried out:

- Thermal analysis and calorimetric studies [1-5] investigate the thermal degradation processes of the plant species. They provide information about the kinetics and the heat released from the combustion of these fuels. The heating rate is generally less than 10 $K.min^{-1}$. Thus, the experimental conditions are far from actual wildfires.
- Static combustion experiments are dedicated to the burning of forest fuel. Species are placed in cylindrical baskets [6-7]. The mass loss, the flame geometry and the temperature distribution are analysed. In these experiments, the prevailing parameter is the surface-to-volume ratio, hiding the influence of the other parameters.
- Different sets of fire propagation in pine needle beds [8-14] are carried out by a lot of authors. These experiments are mainly focused on the determination of the rate of spread under different conditions (wind, slope, fuel characteristics…) and

are used to validate numerical models.

- The last aspect concerns the degradation gases released by forest fuels. Since the pioneering work of Grishin [15], the combustible part of the devolatilization products is considered to be solely carbon monoxide burning in air, whatever the vegetative species. However, these fuels are complex materials and the mixture composition of their degradation gases change with the vegetative species [5].

To our knowledge, the studies at laboratory scale do not allow clearly understanding the coupling between gas and solid phases. Our work is motivated by this statement. It aims to improve the knowledge of heat and mass transfer occurring in the burning of vegetative fuels. As the geometry of a forest fuel plays an important role in its combustion, we choose to decrease the influence of this parameter. Three different species (*Pinus pinaster*, *Erica arborea* and *Cistus monspeliensis*) were crushed and sieved to obtain samples with same mass and particle size. We studied experimentally unsteady, axisymmetric, non-premixed laminar flames resulting from the burning of the samples. These flames bring two main advantages. Firstly, they ensure a good reproducibility of the experiments. Secondly, time-varying laminar diffusion flame is a class of non-premixed combustion [16] bridging the gap between steady laminar combustion and turbulent combustion that is encountered in forest fires. On one hand, the distribution of temperature along the flame, the flame height and the flame radius as well as the mass loss were measured. On the other hand, the thermal properties of the solid phase were obtained by using a differential scanning calorimeter (DSC) and a hot disk technique. The gases released by the degradation of the fuels were determined with a tube furnace connected to a gas chromatograph and to a hygrometer.

The experimental procedures are described in the following section. Next, the global observations of the fuel burning are provided. The behaviour of the solid phase is then

investigated and the gas phase is characterized. Finally, the coupling between the solid phase and the flame is discussed.

2 Experimental devices and methods

2.1 Fuel samples

We studied the burning of three Mediterranean fuels: *Pinus pinaster*, *Erica arborea* and *Cistus monspeliensis* involved in wildland fires. These plants belong respectively to the tree stratum, to the higher shrub layer and to lower shrub layer. They were collected in winter during a period of hydrous stress for vegetation. Before experiments, the plants were oven dried at 60°C for 24 hours and then they were crushed and sieved to a particle size of 0.6-0.8 mm. The geometry of the fuel sample is also equivalent for the three species. The moisture content due to self-rehydration was less than 2 % for all the samples before each burning.

2.2 Time-varying, axisymmetric, diffusion flame

2.2.1 Experimental device

The experimental device is shown in Fig. 1. The fuel samples were in the shape of a cylinder with a diameter of 3.5 cm and a mass of 1.5 g. The depth of the sample depended on the bulk densities of the fuel (ranging from 4 to 5 mm). The combustion set-up was composed of a one square meter plate drilled at its centre. A ten square centimetres insulator was included at this location to support the fuel. It was positioned on a load cell in order to measure the fuel mass loss as a function of time. To insure a fast and homogeneous ignition, a small amount of ethanol (0.7 mL) was spread uniformly on the fuel bed and was ignited with a flame torch. An array of 11 thermocouples was positioned above the fuel bed along the flame axis. The first

thermocouple was placed 1 cm above the top of the support and the others were located 1 cm from each other. A second array of thermocouples was located horizontally movable at different heights to obtain the temperature along the flame radius and inside the vegetative sample. The spacing between these thermocouples was 5 mm. The thermocouples used were mineral-insulated integrally metal-sheathed pre-welded type K (chromel-alumel) pairs of wire with an exposed junction. At the exposed junctions, the wires were 50 μm in diameter. The load cell was chosen for its short response time (0.2 s) compared to the analytical balances which have a response time greater than 3 s. The uncertainty in temperature and mass measurements were respectively 0.5°C and 0.031 g. The sampling frequency was 100 Hz. Two visible cameras were located inside the room (Fig. 1). Camera 1 followed the flame behaviour and the flame height. Camera 2 was placed above the flame in order to record the regression of the flame basis. The ambient temperature was 21°C and the relative humidity was 50 %. At least five repetitions were made to collect reliable data for each fuel.

2.2.2 Image processing

An automatic algorithm was developed in order to follow the flame height and the flame radius (recorded by camera 1 and 2 in Fig. 1) as a function of time during the combustion. Images were first extracted from videos with a sampling rate of 0.5 Hz as the flame is laminar, axisymmetric and does not flicker. This frequency allows reducing the processing time without losing accuracy. For each image, the flame was segmented from the background by using selection criteria based on the RGB (Red, Green and Blue) components. The first step of the pixel extraction was the selection of pixels with a high magnitude in the red component. In the second step, only the pixels with a certain gap between the red and blue components and the red and green components

were kept. This avoided the selection of pixels whose colour is due to light effects. Binary images resulting from this processing clearly show the segmented flame (Fig. 2). Next, the flame height and the radius of the flame basis were computed using the cartesian coordinates of the white area in the image plane. For the frontal view, the height of the flame corresponded to the height of the white area. In the case of top vision, the radius of the flame basis was the average diameter of the white area.

2.3 Geometrical properties of the samples

2.3.1 Bulk density

For determining the bulk densities ρ_{bulk} of the samples, a fixed volume was filled with fuel and weighted. These measurements were repeated ten times. An average of these values was calculated as well as the standard deviation.

2.3.2 Surface-to-volume ratio

The mean surface-to-volume ratio σ of the particles was obtained thanks to a granulometric analysis. A sample of each species was treated by image processing using a high resolution scanner. It provided the mean length and the width of the particles. By assuming that the shape of the particles was a cylinder, the mean surface-to-volume ratios were calculated for each sample thanks to the following relation:

$$\sigma = \frac{2}{L} + \frac{4}{l} \qquad (1)$$

2.4 Physical properties of the samples

2.4.1 Specific heat

The measurements of the specific heat were performed using a differential scanning calorimeter (model DSC Setaram® 131). It is a thermal analysis technique in which the difference in the amount of heat required to increase the temperature of a sample and a reference are measured as functions of temperature. The samples of about 50 mg were placed in an aluminium pan. The experiments were carried out at atmospheric pressure under air flow. In order to determine the specific heat of the samples, a "three-step" method with two pans was used: the same temperature program was applied to each sample, to a reference sample (i.e. zinc) and to an empty pan. The temperature program is based on a stepwise method. Each run consists in successive temperature increments of 20°C performed at 5°C.min^{-1}. After each increment, a waiting period of 5 min is observed to obtain a stable signal. The temperatures ranged from 80 to 200°C what allowed studying the fuel sample just before its thermal degradation. In the "three-step" method, mean specific heat in the range of temperature $\left[T_k, T_{k+1}\right]$ was calculated with the following relationship:

$$C_{p_{mean,sample}}(T_k \rightarrow T_{k+1}) = C_{p_{mean,reference}} \cdot \frac{m_{reference}}{m_{sample}} \cdot \frac{\int_{T_k}^{T_{k+1}} HF_{sample}.dT - \int_{T_k}^{T_{k+1}} HF_{empty}.dT}{\int_{T_k}^{T_{k+1}} HF_{reference}.dT - \int_{T_k}^{T_{k+1}} HF_{empty}.dT} \qquad (2)$$

where HF stands for the heat flow, m is the mass of the sample, C_p represents the specific heat and k is a time increment.

2.4.2 Thermal conductivity

Thermal conductivity measurements were conducted using the hot disk technique [17], which is a transient plane source method. The hot disk technique can be used to measure thermal conductivity in the range of 0.005 W.m^{-1}.K^{-1} to 500 W.m^{-1}.K^{-1}. The hot disk sensor is made of a double spiral of nickel wire. During the experiments, the hot

disk sensor was placed in the fuel bed. A small constant current was supplied to the sensor used as a temperature monitor. The temperature increase in the sensor was accurately determined through resistance measurement. By monitoring this temperature increase over a short period of time after the beginning of the experiment, it is possible to obtain accurate information on the thermal conductivity of the fuel sample. The thermal conductivity measurements were performed for the three species and for two temperatures: 100 and 200°C. The standard error is 5 %.

2.4.3 Density and Fuel packing ratio

For each sample, the density measurement was performed with a graduated test tube of 10 ml. The determination of the density was carried out in three steps. Firstly, a mass of sample (m_{sample}) was placed in the tube test. 3 ml of absolute ethanol ($V_{ethanol}$) was added in the tube. The absolute ethanol ensures the total immersion of the fuel sample in the fluid. Finally, we noted the total volume (V_{total}). The density of the sample is given by:

$$\rho_{sample} = \frac{m_{sample}}{V_{total} - V_{ethanol}} \quad (3)$$

The fuel packing ratio corresponds to the ratio between the bulk density and the density of the fuels. It is given by the relation:

$$\alpha = \frac{\rho_{bulk}}{\rho_{sample}} \quad (4)$$

2.5 Composition of the pyrolysis gases

The tube furnace apparatus used as pyrolyser is shown in Fig. 3. It is made of a cylindrical furnace 43.5 cm long with an internal diameter of 6.5 cm. The reactor inside, is 86 cm long with an inner diameter of 5 cm. Two thermocouples were used to record the temperature history in the furnace. One was fixed on the inner surface of the furnace

and the other was placed in the combustion chamber to follow the temperature in the sample at different height. Experiments were conducted for the three fuels. Thermogravimetric analysis showed that the most important degradation of the sample occurs between 250 and 425°C [18]. We chose to study the degradation gases for this range of temperature. The temperature of the furnace was set at 450°C. This furnace temperature allows the samples attaining the chosen range of temperature. Gases were collected into a balloon called the gas sampler, hereafter. The combustion chamber filled with 4 g of sample was kept outside of the furnace until the temperature of the furnace has reached the required value. At the same time, air suction was switched on, the gas sampler was opened and nitrogen was injected at 1 L/min to obtain an inert atmosphere in the device. Once the temperature was stable, the sample was introduced inside the furnace. The injection of nitrogen was stopped, gas sampler was closed and the valve (8a on Fig. 3) allowing the ejection of gases outside the apparatus was opened. When samples reached the required temperature, gas sampling began. Valve 8a was closed, a gas sampler was opened and nitrogen was injected into the reactor to fill the gas sampler with pyrolysis gases. Then the gas sampler was directly attached either to the gas chromatograph (Flame Ionization Detector and Thermal Conductivity Detector) or to the hygrometer (EdgeTech Model 2001 Series DewPrime) measuring the dew point with a resolution of 0.1°C. The mass loss of the sample between 280 and 425°C was measured for each run. At least three repetitions were carried out. Three tests without fuel were also carried out to verify that there was no leak.

3 Results and discussion

The main objective of this section is to determine the factors that govern the fuel burning. To proceed, we compare the flames resulting from the burning of the three

vegetative species (*Pinus pinaster*, *Erica arborea* and *Cistus monspeliensis*). First of all, we describe the global behaviour of the three flames. Next, the physical and geometrical properties of the solid phase are depicted as well as the temperature in the sample and its mass loss. Then, the composition of the degradation gases and the temperature distribution in the flame are presented. Finally, we underline the coupling between the solid phase and the flame through the study of the flame geometry and the axial temperature.

3.1 Burning experiments

The same global tendency was observed for the burning of the all vegetative species, including three different stages: ignition, laminar flame and extinction. The first stage corresponded to a flickering flame due to the presence of ethanol to ignite the sample. It lasted around 60 s. During the second stage, the ethanol was completely burned and the fuel was only composed of the degradation gases. The flame became laminar. It was absolutely axisymmetric and was slightly conical with a narrow tip (Fig. 2). The flame height and radius decreased slowly. The last stage concerned the extinction of the flame. The remaining solid phase was essentially made up of carbon at the surface of the sample with a certain amount of unburned fuel near the support (Fig. 4). Contrary to the other samples, the remaining solid phase of *Erica arborea* was covered by tar. For the whole species, a small and negligible amount of ashes was observed at the surface too. The combustion time depended on the species. It lasted on average 100 s, 155 s and 170 s for *Cistus monspeliensis, Pinus pinaster* and *Erica arborea* respectively.

3.2 Description of the solid phase

3.2.1 Ultimate analysis

The ultimate analysis of each species is presented in Table 1. The composition in C, H, and O of the samples is close. The main differences concern the ash contents. It is nine times greater for *Cistus monspeliensis* than for *Pinus pinaster*. The inorganic part affects the plant combustion. Some mineral matter, present in the fuel, strongly catalyses the decomposition of cellulose components [19]. High ash contents decrease the volatilisation rate, increase the residue and induce a lower temperature of active pyrolysis [1].

3.2.2 Density

The densities of the sample are 927, 831 and 904 $kg.m^{-3}$ respectively for *Pinus pinaster*, *Erica arborea* and *Cistus monspeliensis*. These values are higher than the uncrushed plants' ones [6] as the crushing breaks the lamina and gaps appear in the spongy mesophyll. For a same mass, the volume of the crushed samples is lower than the uncrushed plants' ones increasing their density.

3.2.3 Surface-to-volume ratio

The mean surface-to-volume ratios of the samples are 6494, 6755 and 7198 m^{-1} respectively for *Pinus pinaster*, *Erica arborea* and *Cistus monspeliensis*. The surface-to-volume ratio of *Cistus monspeliensis* is higher than the two other's ones. In literature [20], the surface-to-volume ratios of the uncrushed plants are very different as they are around 4260 m^{-1} for *Pinus pinaster*, 8200 m^{-1} for *Erica arborea* and 3250 m^{-1} for *Cistus monspeliensis*. The crushing and the sieving allow obtaining samples with a comparable surface-to-volume ratio. The influence of this factor was thus minimized allowing us studying the impact of the other parameters.

3.2.4 Thermal diffusivity

3.2.4.1 Specific Heat

The mean specific heats between 80 and 200°C of the sample are 2017, 1856 and 1834 $J.kg^{-1}.K^{-1}$ respectively for *Pinus pinaster*, *Erica arborea* and *Cistus monspeliensis*. Some little fluctuations were observed during the measurements. They were due to two endothermic reactions:

- The vaporization of the water due to the self-rehydration of the fuel that occurs around 100°C.
- The release of volatile organic compounds like terpenic molecules [21], which are released below the pyrolysis temperature [22].

However, the influence of these endothermic reactions can be neglected as, during this range of temperatures, the specific heat varies slightly around the mean value. The standard deviation is less than 5 %. The specific heat of the three species is roughly the same. The specific heats of *Erica arborea* and *Cistus monspeliensis* are very close whereas the *Pinus pinaster* one is slightly higher. In literature, few data concerning vegetal fuel are reported apart from wood. The specific heat of dry wood depends on temperature and is given by [23]:

$$C_{p_{drywood}} = 103.1 + 3.867T \qquad (5)$$

Thus, the specific heat of dry wood is 1545 and 1932 $J.kg^{-1}.K^{-1}$ respectively at 100 and 200°C. These value are close from our results.

3.2.4.2 Bulk density

The bulk densities of the crushed samples are 365, 376 and 298 $kg.m^{-3}$ respectively for *Pinus pinaster*, *Erica arborea* and *Cistus monspeliensis.* The mean standard deviation is less than 3.2 %. The measurements are quite reproducible. According to the values of the density and to the bulk density, the fuel packing ratio is 39 % for *Pinus pinaster*, 45% for *Erica arborea* and 33 % for *Cistus monspeliensis.* In the experiments carried out at laboratory scale for fire across pine needles [11-14], the fuel packing ratio of the pine litters is about 3 %.

3.2.4.3 Thermal Conductivity

Table 2 shows the thermal conductivities of the samples at 100 and 200°C. The standard deviation is 0.002. For the three fuels, the thermal conductivities are low (less than 0.2 $W.m^{-1}.K^{-1}$) and close. For the two temperatures, the thermal conductivity of *Erica arborea* is slightly higher than respectively *Pinus pinaster* and *Cistus monspeliensis*'s one. Between 100 and 200°C, the change of thermal conductivity is essentially due to the vaporization of the water and the release of volatile organic compounds. At this range of temperature, the thermal conductivities change little. Like for the specific heat, these two reactions can be neglected. While significant literature has been reported on thermal conductivity of wood, little has been reported on other vegetal fuel. The values obtained for wood are close to our results [24]. For the three samples, the thermal conductivity seems to be linked with the fuel packing ratio. For a same temperature, the sample with the highest fuel packing ratio exhibits the highest thermal conductivity. This tendency is reported in Suleiman *et al.* too [25].

3.2.4.4 Thermal Diffusivity

The thermal diffusivity (noted a) is given by the relation:

$$a = \frac{\lambda}{\rho_{bulk}.C_p} \quad (6)$$

Table 3 presents the thermal diffusivities at 100 and 200°C for the three samples. For both temperatures, the highest thermal diffusivity is obtained for *Cistus monspeliensis* followed by *Erica arborea* and by *Pinus pinaster*. Thus, between 100 and 200°C, the temperature change in the sample of *Cistus monspeliensis* will appear quickly than for the other species. For the vegetal char, the thermal diffusivity can be assumed to be the same as that of graphite. The chars of the three plants have also the same thermal diffusivity. At 400°C, for graphite char, the specific heat is 1513 $J.kg^{-1}.K^{-1}$, the thermal conductivity is 0.620 $W.m^{-1}.K^{-1}$ and the bulk density is 120 $kg.m^{-3}$ [26]. The thermal diffusivity is also equal to $8.3\ 10^{-3}\ m^2.s^{-1}$. The raise of temperature of char is also quicker than the unburned sample's one.

3.2.5 Sample temperature

The sample temperature was determined thanks to the horizontal array of thermocouples placed on the vegetative sample (Fig. 2). For the three fuels, the surface temperature follows the same trend. We only present the mean surface temperature of *Pinus pinaster* (Fig. 5) from five experiments. Around 10 s, the temperature is maximal at 1.5 cm from the centre. It coincides with the reaction zone of the flame. At this moment, the remaining part of the surface is heated by radiation leading to a linear temperature increase. After 20 s, the reaction zone of the flame moves to the centre and the temperature decrease at 1.5 cm. At 80 s, the reaction zone of the flame arrives at 1 cm from the centre. The same trend appears: the temperature reaches a maximum and then

decreases with the radius reduction. Thus, the evolution of the surface temperature highlights the regression of the flame base during the burning.

Inside the sample, the temperature increases differently according to the fuel. Figures 6.a. to c. present the mean temperature along the depth of the sample at 5 mm from the centre for the three species. We can observe a propagation of the heat wave in the sample. The particles are heated by conduction from the surface to the bottom. Below 200°C, the sample does not degrade. Thus, for the whole species, near the support, the sample temperature is not sufficient so that the sample degrades. This observation explains the presence of the unburned fuel at this place (Fig. 4). For *Pinus pinaster*, only the particles located on the first millimetre under the surface have a sufficient temperature to degrade. For *Erica arborea* and for *Cistus monspeliensis,* the sample degrades over the two first millimetres. However, the temperature recorded at 1 mm under the surface is higher for *Cistus monspeliensis* than for *Erica arborea.* Thus, the heat diffusion is more significant in the sample depth for *Cistus monspeliensis* than respectively for *Erica arborea* and *Pinus pinaster.* This behaviour is in agreement with the thermal diffusivities of the samples (Table 3) as the thermal diffusivity of *Cistus monspeliensis* is greater than *Erica arborea*'s and *Pinus pinaster*'s ones.

3.2.6 Mass loss

The load cell allowed obtaining the evolution of the mass loss for the three samples. The mean mass loss was calculated from five experiments and approximated by 4th order polynomials (Fig. 7.a.). The global mass loss of the samples is 0.14, 0.25 and 0.15 g respectively for *Pinus pinaster, Erica arborea* and *Cistus monspeliensis*. It corresponds to a percentage between 10 and 18 % of the combustible part of the samples (sample mass minus ash proportion).

During the ignition stage, the most significant mass loss is observed for *Cistus monspeliensis* followed by *Erica arborea* and *Pinus pinaster*. The combustion of *Cistus monspeliensis* stops quickly in the laminar stage whereas the mass loss of the two other samples goes on. This difference of combustion dynamics is mainly due to the surface-to-volume ratio of *Cistus monspeliensis*'s particles. As said previously, a high surface-to-volume ratio involves a most efficient absorption of the radiative heating leading to a quickest combustion [6]. Thus, for *Cistus monspeliensis*, the crushing and sieving of the leaves was not sufficient to decrease the effect of the surface-to-volume ratio. This result shows the interest to crush and sieve the vegetative fuels to observe the impact of the other physical properties on their combustion. The difference of surface-to-volume ratio between *Erica arborea* and *Pinus pinaster* is less substantial. Although this parameter could influence the solid behaviour, the difference of mass loss occurring during the ignition stage may be due to the ash content. For *Erica arborea*, it is four times higher than *Pinus pinaster*'s one. As seen previously [1], the pyrolysis of *Erica arborea* begins also at lower temperature than *Pinus pinaster*'s one. It entails a more significant mass loss of *Erica arborea* during the ignition stage.

During the laminar phase, others factors control the mass loss of the samples. Figure 7.b. presents the mean mass loss rate for the three fuels during this stage, approximated by 3rd order polynomials. The mass loss rates of *Cistus monspeliensis* are lower than the two other ones as this sample finishes its burning. Although that the thermal degradation occurs deeper in the sample of *Erica arborea* (Fig. 6), the mass flow rate of degradation gases of *Erica arborea* and of *Pinus pinaster* are close. The degradation of *Erica arborea*'s sample produces more tar, which settles on the sample surface reducing its mass loss

The mass loss is piloted by the surface-to-volume ratio. However, for a same surface-to-volume ratio, the mass loss is linked to the ash content, to the sample temperature and to the production of tar.

3.3 Description of the gas phase

3.3.1 Degradation gases

Table 4 shows the degradation gases analysed for the three fuels. Degradation gases mainly consist of CO_2, CO, CH_4, O_2, H_2O, C_4H_6 and lower amounts of C_2 and C_4 hydrocarbons. These results are in agreement with the literature [15]. Hemicellulose degrades between 200 and 300°C [27] and contributes weakly to the composition of degradation gases occurring during the range of temperature studied here (280 to 425°C). Cellulose is mainly responsible for the production of flammable volatile gases [28]. Between 300 and 350°C, the formation of tar vapour from cellulose becomes predominant due to the decrease of its degree of polymerization. A deposit of tar on the reactor outside the furnace confirms this result. The degradation of lignin occurs between 225 and 450°C. Although it produces some volatile gases, lignin is mainly responsible for the char formation [29]. Thus, the degradation gases come mainly from cellulose [30].

3.3.2 Radial temperature

As the radial temperatures follow the same trend for the three species, we only present the mean radial temperatures at 1 cm high for *Erica arborea* (Fig. 8.a.). During the first 60 s, the curves fluctuate due to the ignition with ethanol, then, they become smooth during the laminar stage. The maxima correspond to the crossing of the thermocouples by the reaction zone. As the flame height and radius decrease, these maxima move to

the centre of the samples. Fig. 8.b. shows the mean radial temperature at 1 cm high at 60, 110 and 160 s. As the flame comes through the array of thermocouples, the temperature distribution obtained on Fig 8.b. is characteristic to the profile obtained for a diffusion flame [31].

3.3.3 Vertical temperature

Like for the radial temperature, the vertical temperatures follow the same trend for the three species. The mean time evolution of temperature for thermocouples number 1, 2, 3, 4, 5, 7 and 11 are presented in Fig. 9 for *Erica arborea*, as they are representative of the fire plume. The first stage of the flame (presence of alcohol) lasts approximately 60 s and will not be considered in the following. At the beginning of the second stage, thermocouples 1 to 5 take place inside the laminar flame, while the others (thermocouples 7 and 11) are located above it. The maximum temperature observed in the flame is around 1000°C. As the flame decreases during this stage, thermocouples 1 to 3 remain wrapped up in the flame. Thermocouples 4 and 5 cross the flame during its regression recording successively the temperature of the reaction zone and that of the thermal plume. The temperature decreases progressively from 800°C to the ambient. The temperature recorded by the upper thermocouples (thermocouples 7 and 11) decrease slowly from 600°C to the ambient with more fluctuations, since the flow becomes progressively turbulent in the thermal plume.

3.4 Coupling between the solid phase and the flame

The coupling between the solid phase and the flame can be particularly highlighted by two variables: the flame geometry and the temperature distribution.

3.4.1 Flame geometry

The geometrical description of the flame was managed with two visible cameras (Fig. 1). Fig. 10 shows the visible radius of the flame base versus mass flow rate. The flame radius of *Cistus monspeliensis* decreases linearly with the mass flow rate. For the two other species, the radius decrease is slow for high mass flow rate. But, when the mass flow rate reduces, the regression of the flame base is more significant. For a given flow rate, the flame radius of *Cistus monspeliensis* is smaller than the other's one. Figure 11 presents the visible flame height versus the mass flow rate of the degradation gases. These curves can be approximated by a straight line. For *Cistus monspeliensis*, the slope of the curve changes for heights lower than 0.5 cm. This part of the graph corresponds to the flame extinction. Contrary to the two other species, the flame extinction of *Cistus monspeliensis* is gradual. According to Fig. 11, the flame height and the mass flow rate of the degradation gases are also proportional. This observation was made by Jost [32] too. The highest coefficient of proportionality is obtained for *Pinus pinaster* followed by *Erica arborea* and *Cistus monspeliensis*. Around 3 10^{-6} $kg.s^{-1}$, the flames *of Pinus pinaster* and *Erica arborea* have the same mass flow rate and the same flame radius (Figure 10), but have different flame height. Thus, the flame height is proportional to the mass flow rate but also depends on the degradation gas composition as explained in the following.

3.4.2 Temperature distribution

Figure 12 presents the mean temperature at 1 cm high versus the mass flow rate of the degradation gases. We reversed the abscissa axis to follow the chronology of the experiments (high mass flow rates correspond to the beginning of the laminar stage).

The curves of *Erica arborea* and *Pinus pinaster* are close whereas *Cistus monspeliensis*'s one differs. In these graphs, we can distinguish three regions:

- For the highest mass flow rates (until 2, 1.5 and 0.5 10^{-6} $kg.s^{-1}$ respectively for *Pinus pinaster, Erica arborea* and *Cistus monspeliensis)*, the thermocouple at 1 cm high is in the fuel rich zone where an oxygen deficit appears. When the flow rate decreases, the flame approaches thermocouple and the temperature increases steadily. For a same flow rate, the gas temperature of *Cistus monspeliensis* is higher than *Erica arborea*'s one and *Pinus pinaster*'s one.

- For a mass flow rate of 2, 1.5 and 0.5 10^{-6} $kg.s^{-1}$ respectively for *Pinus pinaster, Erica arborea* and *Cistus monspeliensis*, the thermocouple hits the combustion zone. The mean temperature is maximal and is around 1000°C for the three fuels. The heating value per mass of air is calculated from the composition of degradation gases (Table 4) thanks to the following relation:

$$\Delta h_a = \Delta h.f_s \quad (7)$$

where Δh is the reaction enthalpy of degradation gases (7.95, 5.53 and 7.68 $MJ.kg^{-1}$ respectively for *Pinus pinaster, Erica arborea* and *Cistus monspeliensis*) and where f_s corresponds to the stoechiometric coefficient in air (0.43, 0.61 and 0.44 respectively for *Pinus pinaster, Erica arborea* and *Cistus monspeliensis*). The heating value per mass of air calculated for each gas composition is 3.43, 3.40 and 3.40 $MJ.kg_{air}^{-1}$ respectively for *Pinus pinaster, Erica arborea* and *Cistus monspeliensis.* Although the reaction enthalpies of the degradation gases are very different, the heating values per mass of air are close for the three fuels as the reaction is piloted by the available dioxygen during the

combustion. These values explain the weak differences of maximal temperature in flames.

- After the last range of mass flow rate, the temperature decreases as the thermocouple is up to the reaction zone, at the beginning of the thermal plume.

Figure 13 presents the mean axial temperature versus the vertical position for *Pinus pinaster* and *Erica arborea* for a mass flow rate equal to 3 10^{-6} $kg.s^{-1}$. We remind that at this mass flow rate, the two species have the same flame radius (Figure 10). The two curves have the same maximal temperature. However, the temperature profiles are different. The combustion of *Pinus pinaster* appears closer to the surface sample than *Erica arborea*'s one. The combustion kinetics is also different and depends on the composition of degradation gases. In the thermal plume, the temperature decrease is identical for the two species. The temperatures are controlled by the radiation losses in the lower part and by the mixing of burnt gases with air in the upper part.

Thus, the temperature distribution recorded by the thermocouples is linked to the mass flow rate. Although the maximal temperatures are close for the whole species, their combustion kinetics varies following the composition of their degradation gases.

4 Conclusions

In this study, we characterised the physical properties and the degradation gases of crushed vegetative fuels. Their burning was investigated pointing out the coupling between the flame and the solid phase. The main contributions of this work can be summarized as follows:

In the solid phase, the mass loss depends on:

- The surface-to-volume ratio. We decreased its influence by using crushed samples but it showed to have a strong effect, even with small variations.
- The temperature of the whole sample, which releases on the thermal diffusivity.
- The ash content of the plants and the tar production.

In the gas phase:

- Six main gases were identified during the thermal degradation of fuels: CO, CH_4, CO_2, O_2, H_2O and C_4H_6.
- The maximal temperature in the flames is roughly the same for the three species as the heating values per mass of air are close.
- The temperature profiles vary among species in the flame where the combustion kinetics changes following the composition of degradation gases. The differences inside the thermal plume are less important because of the radiation losses and the mixing of burnt gases with air.

Concerning the coupling between the phases:

- The flame height is proportional to the mass flow rate
- There is a non-negligible contribution of the degradation gases.

These results provide fundamental data that can be included in physical models of wildland fires. The flame height, the maximal temperature and the heating values per mass of air can be used in global approaches to depict flames. In multiphase models, the gas and the solid phase are described in details to represent the whole physical mechanisms. This study brings useful experimental data for such models concerning the fuel properties, the mass burning rate and the composition of the pyrolysis products.

To go further into the characterization of the coupling between gas and solid phases in forest fires, other studies are necessary about both the kinetics of fuel degradation and the flame description in particular in turbulent condition.

5 References

[1] Philpot C.W., Influence of mineral content on the pyrolysis of plant materials, Forest Science, 16 (1970) 461-471.

[2] Ghetti P., Ricca L., Angelini L., Thermal analysis of biomass and corresponding pyrolysis products, Fuel 5 (1996), 565–573.

[3] Dimitrakopoulos A.P., Thermogravimetric analysis of Mediterranean plant species, J. Anal. Appl. Pyrolysis, 60 (2001) 123–130.

[4] Leroy V., Cancellieri D., Leoni E., Thermal degradation of lingo-cellulosic fuels: DSC and TGA studies, Thermochim. Acta, 451 (2006) 131-136.

[5] Klose W., Damm S., Wiest W., Pyrolysis and Activation of Different Woods– Thermal Analysis (TG/EGA) and Formal Kinetics, Proc. Int. Symp. of Catal. and Thermochem. Conv. of Nat. Org. Polym., 4 (2000) 9-17.

[6] Dupuy J.L., Maréchal J., Morvan D., Fires from cylindrical forest fuel burner: combustion dynamics and flame properties, Combustion and Flame, 135 (2003) 65-76.

[7] Saâdaoui M., Mahjoub Saïd N., Mhiri H., Caminat Ph., Le Palec G. Bournot Ph., Study of the behaviour of a flame resulting from the combustion of pine needles in a cylindrical basket, Int. J. Therm. Sci., in press (2007).

[8] Rothermel R.C., Anderson H.E., Fire spread characteristics determined in the laboratory. USDA For. Serv. Res. Pap. INT-30, Ogden, Utah, 1966

[9] Anderson H.E., Predicting wind-driven wild land fire size and shape. USDA For. Serv. Res. Pap. GTR-INT-305, 1983

[10] Viegas D.X. , Convective processes in forest fires, Proc. NATO Adv. Study Institute on Buoyant Convective in Geophysical Flows, Kluwer, (1998) 401-420

[11] Dupuy J.L., Slope and fuel load effects on fire behaviour: Laboratory experiments in pine needless fuel beds, Int. J. Wildland Fire, 5 (1995) 153-164.

[12] Catchpole W.R., Catchpole E.A., Rothermel R.C., Morris G.A., Butler B.W., Latham D.J., Rate of spread of free-burning fires in woody fuels in a wind tunnel., *Comb. Sci. Tech.,* 131 (1998), 1-37.

[13] Mendes-Lopes J.M.C, Ventura J.M.P., Amaral J.M.P., Flame characteristics, temperature-time curves and rate of spread in fires propagating in a bed of Pinus pinaster needles, Int. J. Wildland Fire, 12 (2003) 67-84.

[14] Marcelli T., Santoni P.A., Simeoni A., Leoni E., Porterie B., Fire spread across pine needle fuel beds : characterization of temperature and velocity distributions within the fire plume, Int. J. Wildland Fire, 13 (2004) 37-48.

[15] Grishin, A. M., Gruzin, A. D., and Zverev, V. G., Study of the structure and limits of propagation of the front of an upstream forest fire, Fizika Goreniya i Vzryva, 21 (1985) 11-21.

[16] Mohammed, R.K. Tanoff, A. Smooke, M.D. Schaffer, A.M. and Long, M.B., Computational and experimental study of a forced, time-varying, axisymmetric, laminar diffusion flame, Proc. Combust. Inst., 27 (1998) 693-702.

[17] Gustafsson S.E. Transient plane source techniques for thermal conductivity and thermal diffusivity measurements of solid materials, Rev. Sci. Instrum., 62 (1991) 797-804.

[18] Safi M.J., Mishra I.M., Prasad B., Global degradation kinetics of pine needles in air, Thermochim. Acta, 412 (2004) 155-162.

[19] Várhegyi G., Jerry Antal Jr. A., Jakab E., Piroska S., Kinetic modelling of biomass pyrolysis, J. Anal. Appl. Pyrolysis, 42 (1997) 73–87.

[20] Cohen M, Cuinas P, Diez C, Fernandes P, Guijarro M, Moro C, FIRE STAR: a decision support system for fuel management and fire hazard reduction in

Mediterranean wildland - urban interface. Wildland fuel particles characterisation: Database Content. D6-03 Annexe 1, 2003

[21] Owen S., Boissard C. , Hewitt C.N., Volatile organic compounds (vocs) emitted from 40 mediterranean plant species: Voc speciation and extrapolation to habitat scale, Atmos. Environ., 35 (2001) 5393–5409.

[22] Isidorov V.A., Vinogorova V.T. Rafalowski K., HS-SPME analysis of volatile organic compounds of coniferous neddle litter, Atmos. Environ., 37 (2003) 4645–4650.

[23] Ragland K.W., Aerts D.J., Baker A.J., Properties of wood for combustion analysis, Bioresour. Technol., 37 (1991) 161-168

[24] Gupta M., Yang T., Roy C., Specific heat and thermal conductivity of softwood bark and softwood char particles, Fuel, 82 (2003) 919–927.

[25] Suleiman BM, Larfeldt J, Leckner B, Gustavsson M., Thermal conductivity and diffusivity of wood, Wood Sci Technol, 33 (1999) 465-473.

[26] Kanury A.M., Blackshear P. L., Some considerations pertaining to the problem of wood burning, Combustion Science and Technology, 1 (1970) 339-355.

[27] White, R.H. Dietenberger, M.A. Wood Products: Thermal Degradation and Fire, Encyclop. of Mat. Sci. and Technol., (2001) 9712-9716.

[28] LeVan S.L, Thermal degradation, Concise Encyclopedia of Wood and Woodbased Materials, Pergamon, New York, 1989.

[29] Orfão, J.J.M Antunes, F.J.A. and Figueiredo, J.L. Pyrolysis kinetics of lignocellulosic materials—three independent reactions model, Fuel, 78 (1999) 349-358.

[30] Alén R., Kuoppala E., Oesch P., Formation of the main degradation compound groups from wood and its components during pyrolysis, J. Anal. Appl. Pyrolysis, 36 (1996) 137–148.

[31] Williams F.A., Combustion Theory, Addison-Wesley Publishing Company, Redwood City, 1985.

[32] Jost W., Explosion and combustion processes in gases, McGraw-Hill, 1946.

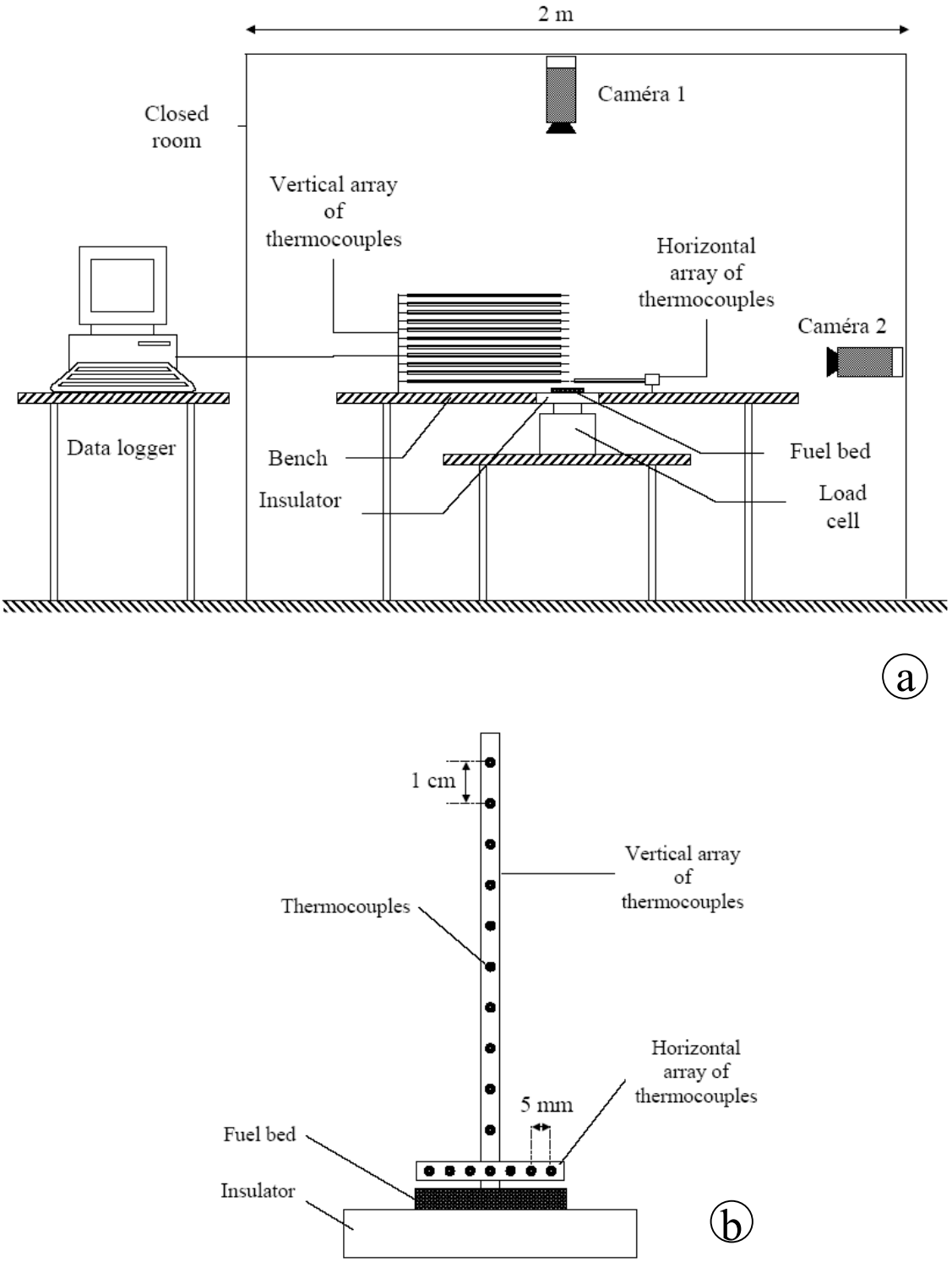

Fig. 1. Sketch of the experimental apparatus – a) Global view – b) Side view.

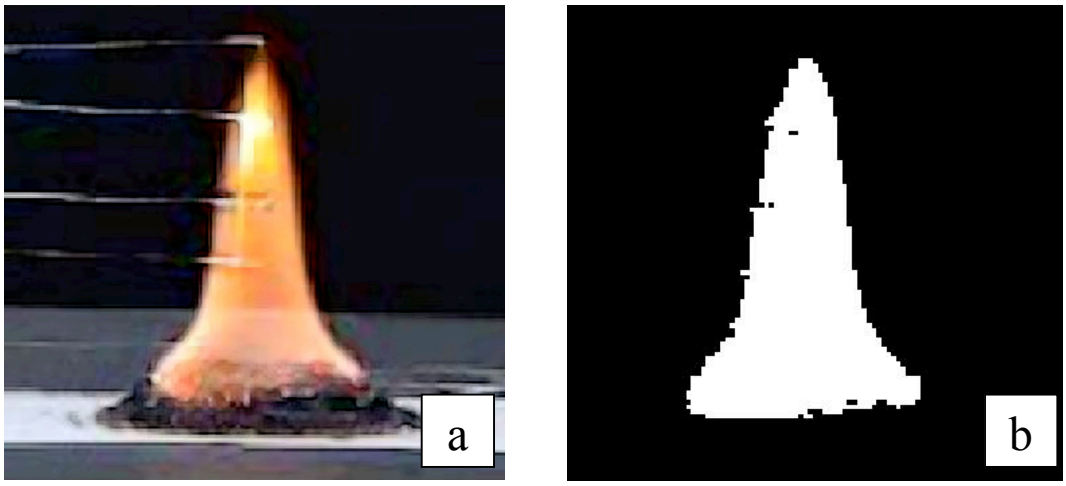

Fig. 2. Image processing – a) Image extracted from the movie – b) Binary image.

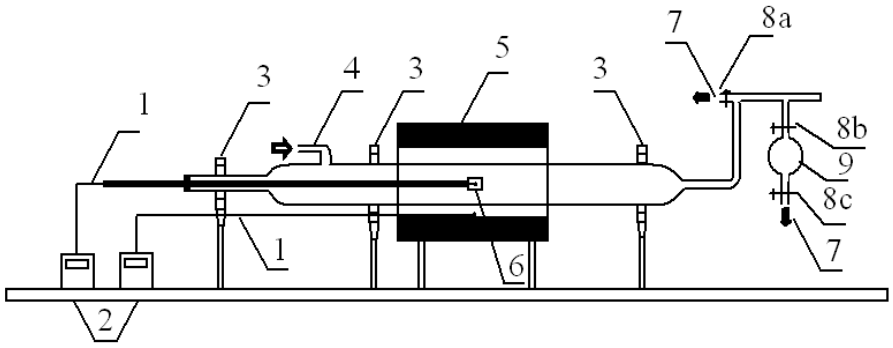

Fig. 3. Schematic of the tube furnace (1 thermocouple, 2 temperature controller, 3 bearing, 4 nitrogen injection, 5 electric furnace, 6 combustion boat, 7 air suction, 8a-c valves, 9 gas samplers).

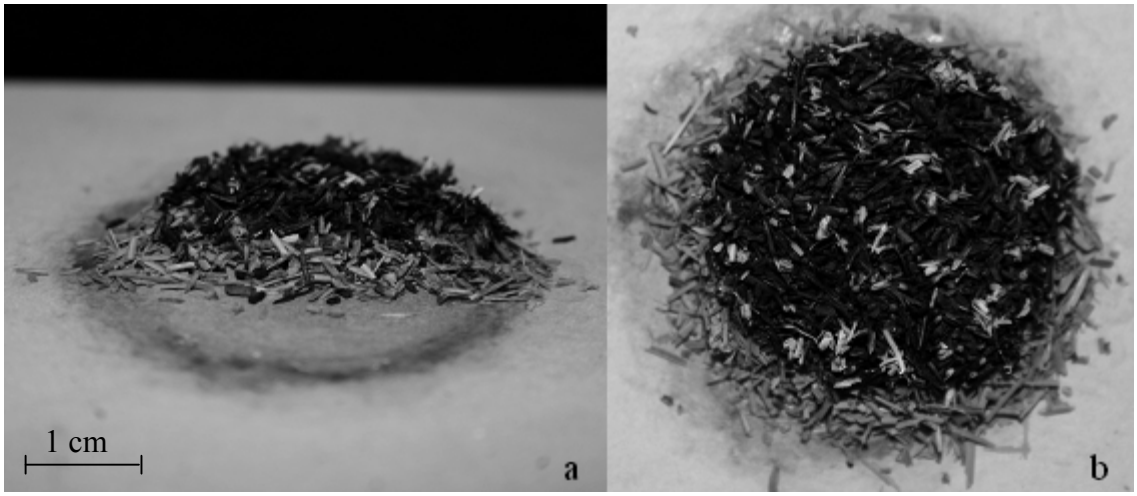

Fig. 4. The remaining solid phase after extinction for *Pinus pinaster* – a) cut-away view – b) top view.

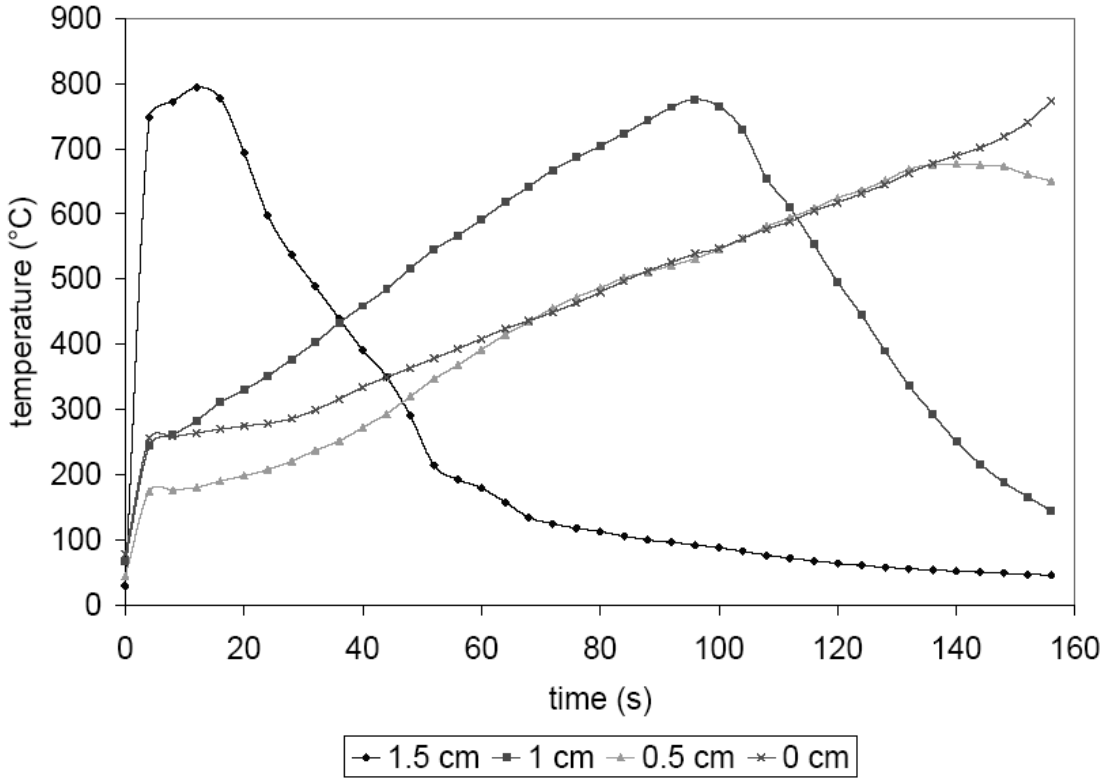

Fig. 5. Temperature of *Pinus pinaster* on the surface sample.

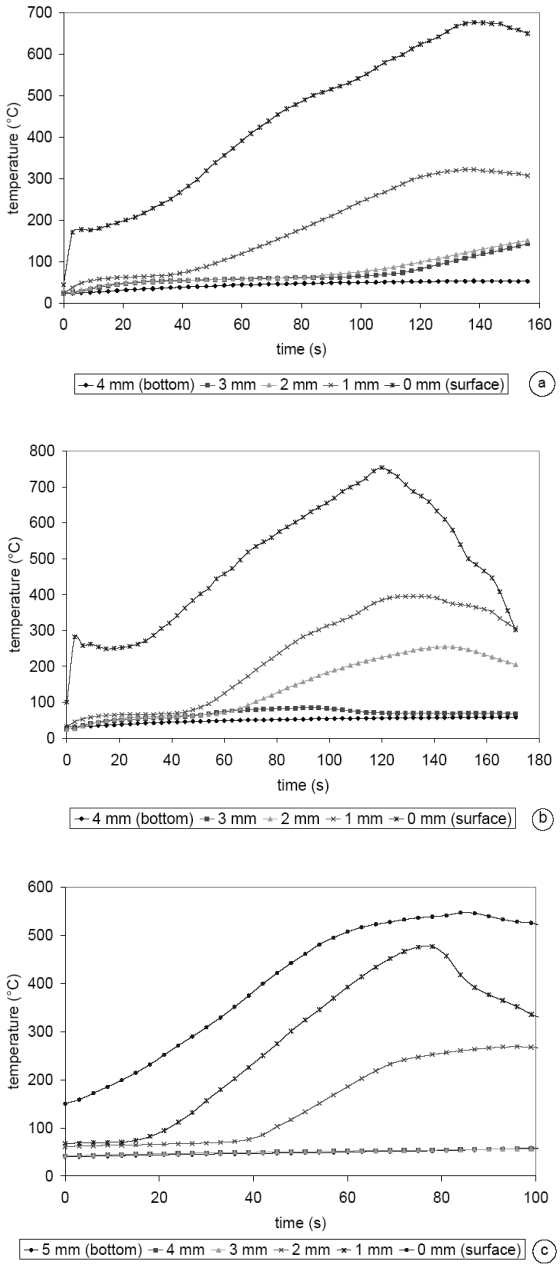

Fig. 6. Temperature along the depth of the sample at 5 mm from the centre for – a) *Pinus pinaster* – b) *Erica arborea* – c) *Cistus monspeliensis.*

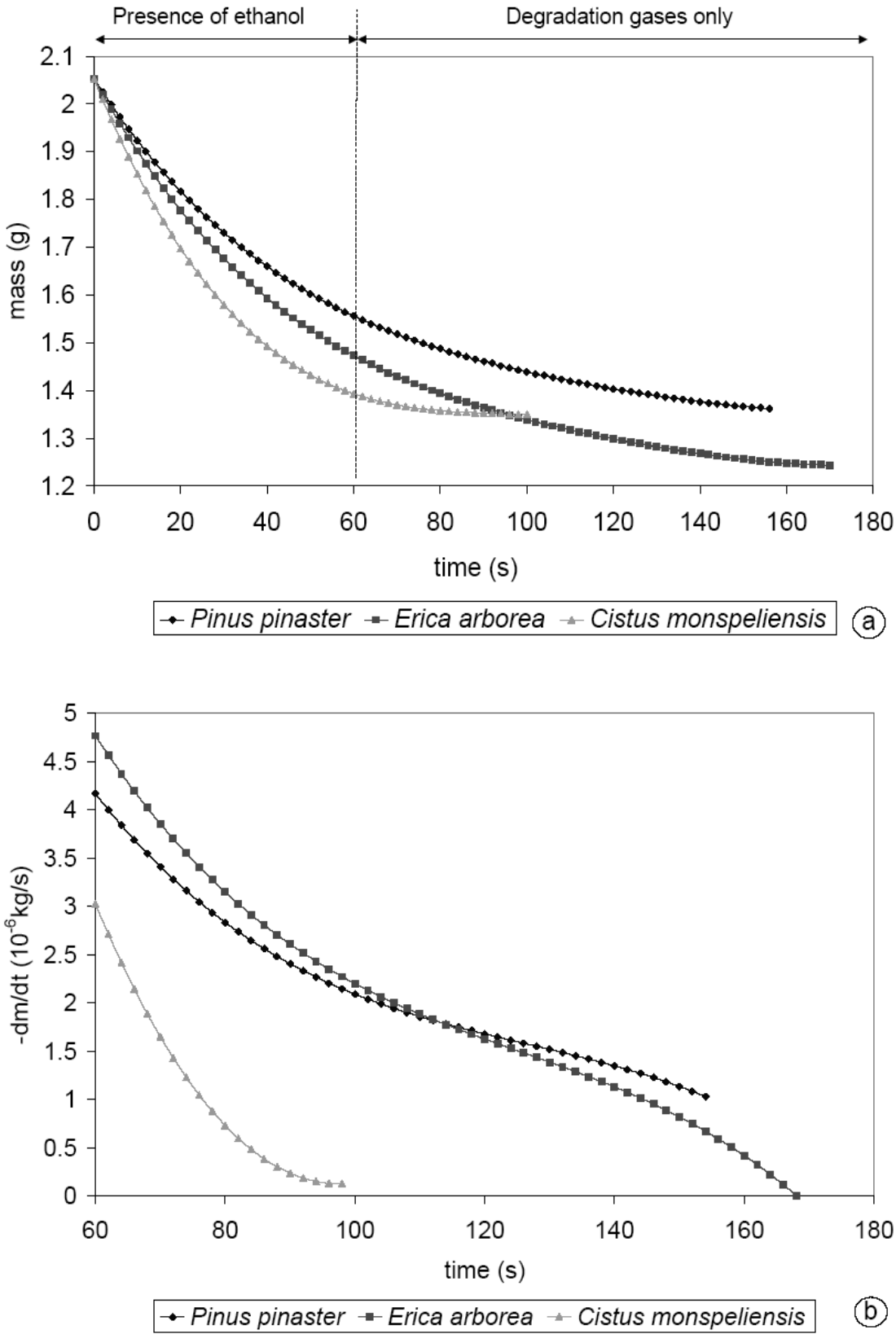

Fig. 7. – a) Mean mass loss for the three fuels – b) Mean mass loss rate for the three fuels.

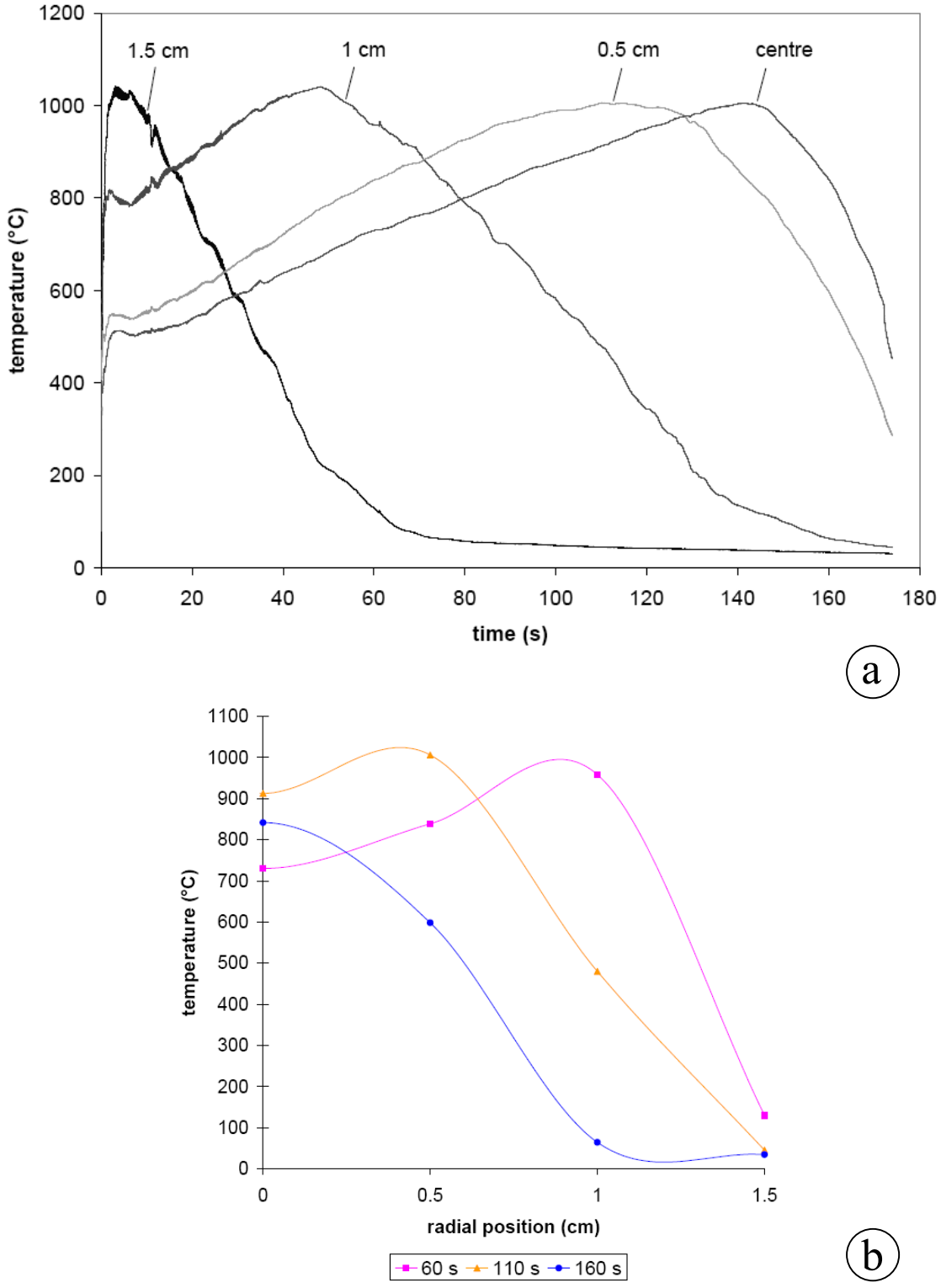

Fig. 8. Mean radial temperatures at 1 cm high for *Erica arborea* – a) versus time.– b) versus the radial temperature for different times.

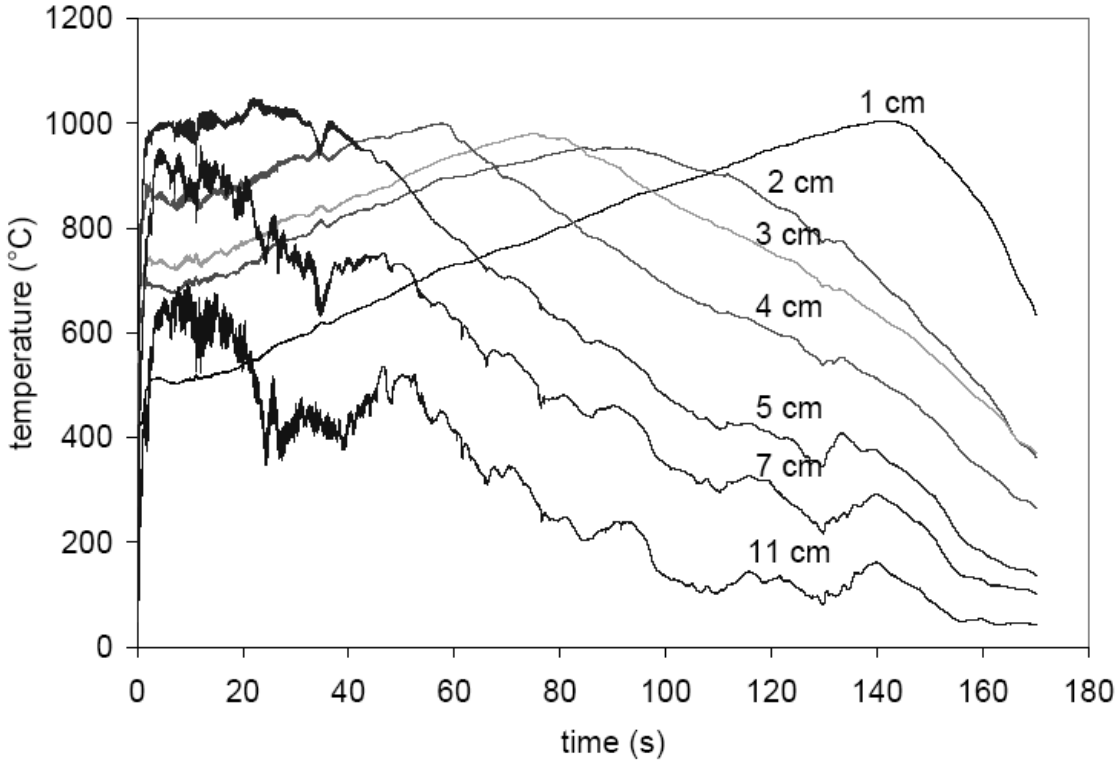

Fig. 9. Mean temperatures along the flame axis for *Erica arborea*.

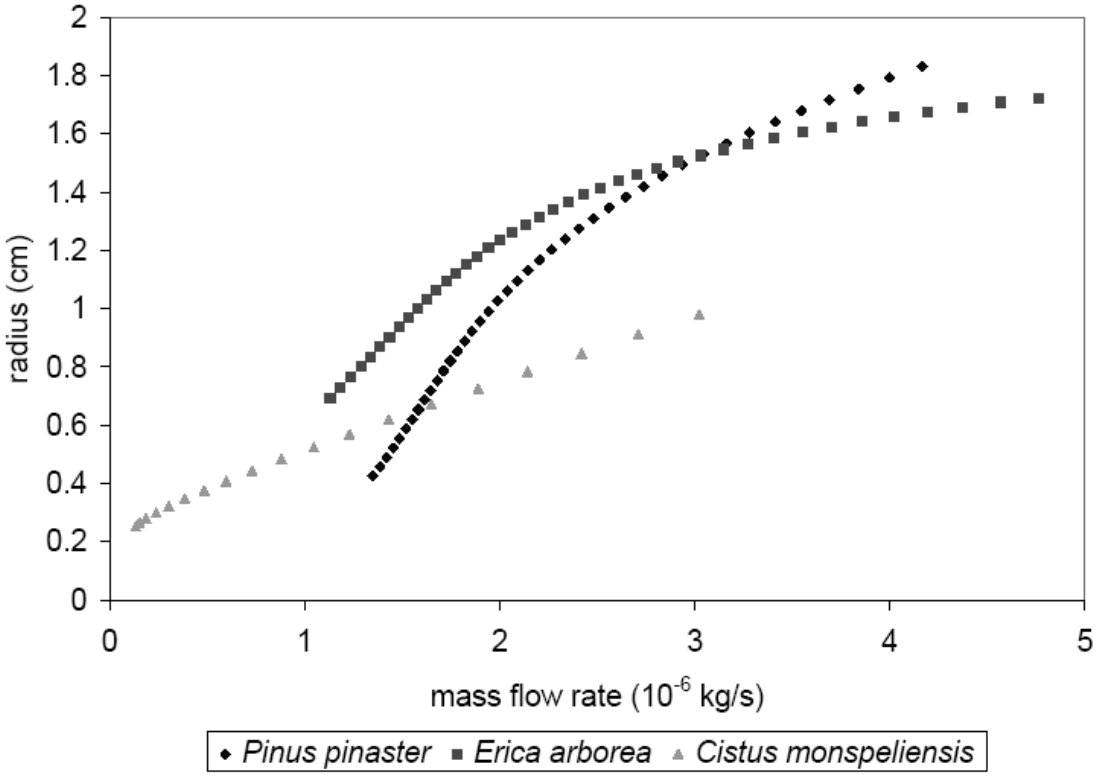

Fig. 10. Visible flame radius versus mass flow rate of degradation gases.

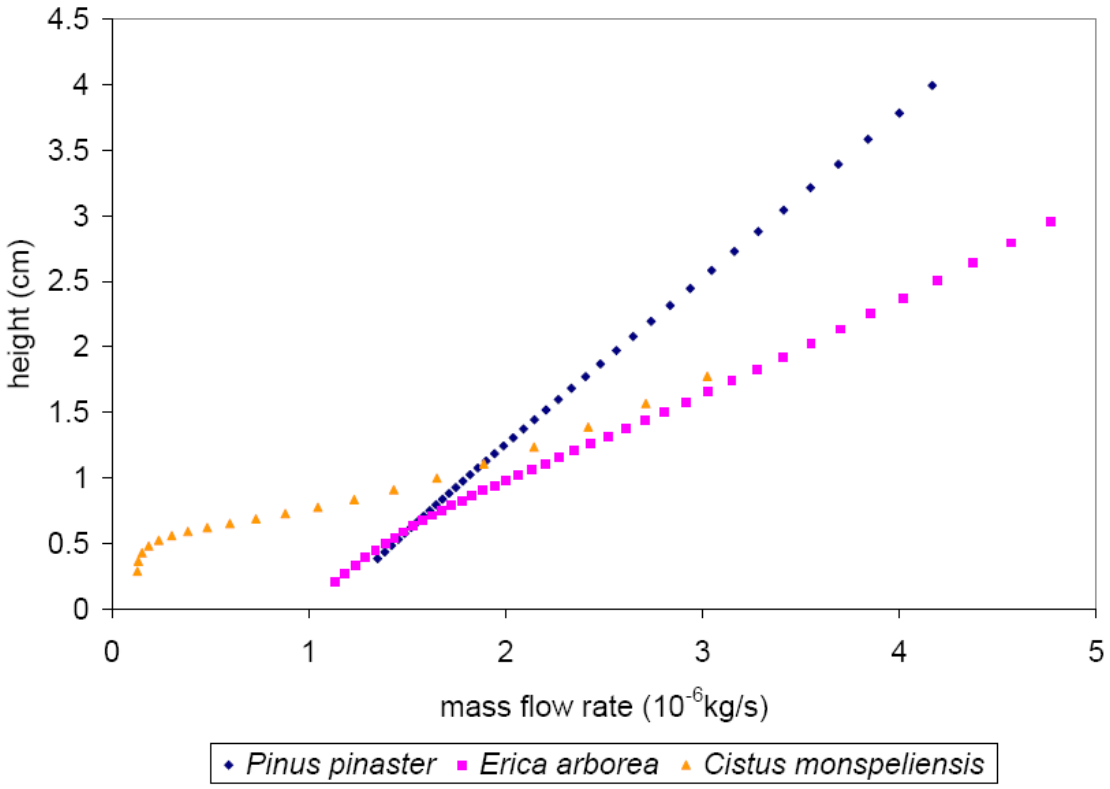

Fig. 11. Visible flame height versus mass flow rate of degradation gases.

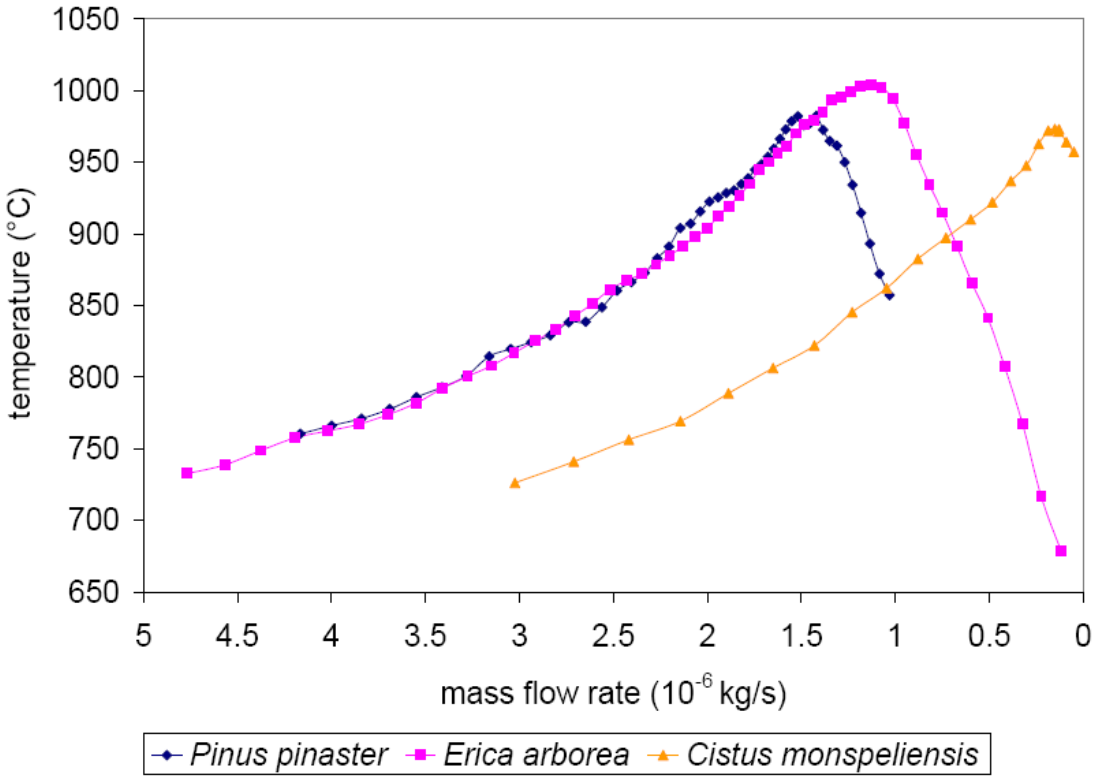

Fig. 12. Mean temperature along the flame axis and at 1 cm versus the mass flow rate of the degradation gases.

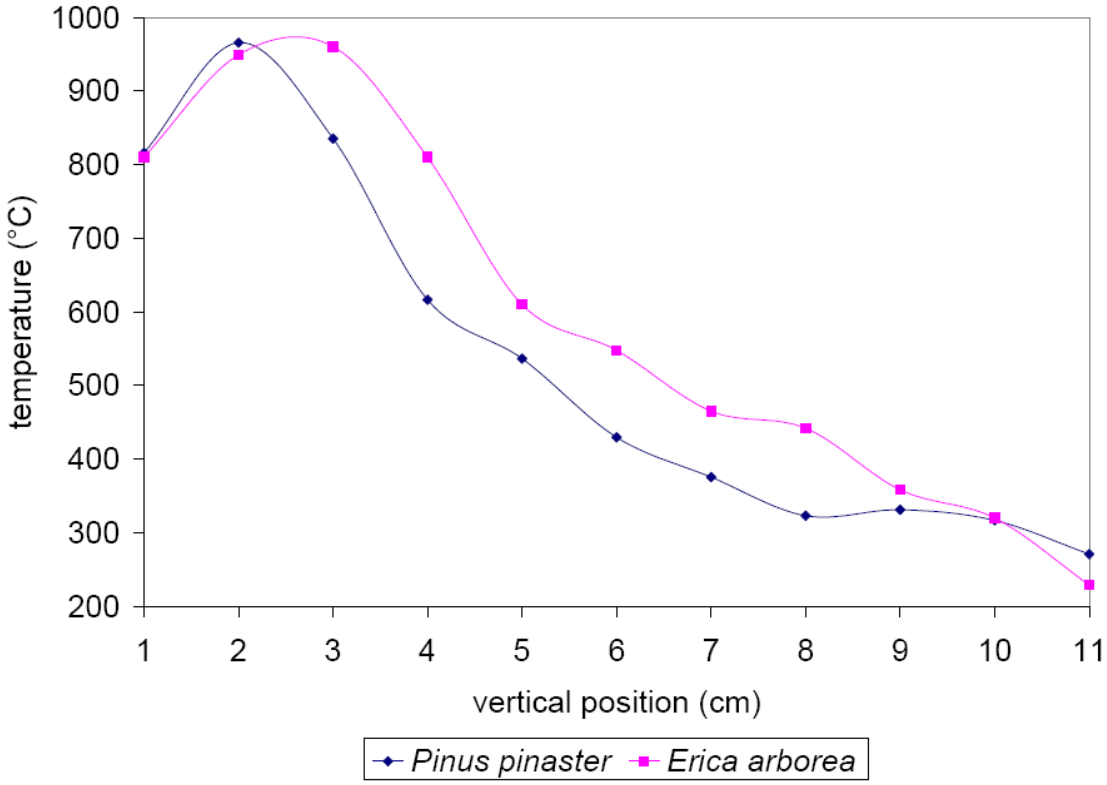

Fig. 13. Mean temperature along the flame axis versus the vertical position for *Pinus pinaster* and *Erica arborea* and for a mass flow rate equal to 3 10^{-6} kg.s^{-1}.

Table 1. Ultimate analysis of three fuels (Wt. %).

Elements / Fuel	C	H	O	Ash
Pinus pinaster	50.64	6.76	41.53	1.07
Erica arborea	52.43	6.98	35.92	4.67
Cistus monspeliensis	46.58	6.22	37.68	9.52

Table 2. Thermal conductivities for the three samples.

Thermal conductivity ($W.m^{-1}.K^{-1}$)		
Temperature (°C) / Species	100	200
Pinus pinaster	0.112	0.119
Erica arborea	0.115	0.119
Cistus monspeliensis	0.107	0.115

Table 3. Thermal diffusivities for the samples.

Thermal diffusivity ($m^2.s^{-1}$)		
Temperature (°C) / Species	100	200
Pinus pinaster	$1.52\ 10^{-7}$	$1.62\ 10^{-7}$
Erica arborea	$1.65\ 10^{-7}$	$1.71\ 10^{-7}$
Cistus monspeliensis	$1.96\ 10^{-7}$	$2.1\ 10^{-7}$

Table 4. Mass fractions of the main pyrolysis gases released by the degradation of the three samples.

Fuel / Gas	*Pinus pinaster*	*Erica arborea*	*Cistus monspeliensis*
O_2	0.028	0.013	0.034
CO	0.187	0.139	0.122
CO_2	0.566	0.713	0.567
CH_4	0.033	0.020	0.033
C_2H_4	0.007	0.004	0.007
C_2H_6	0.012	0.006	0.009
C_3H_6	0.001	0.001	0.004
C_3H_8	0.008	0.005	0.010
C_4H_6	0.048	0.039	0.049
C_4H_8	0.016	0.009	0.018
C_4H_{10}	0.004	0.003	0.008
H_2	0.000	0.000	0.000
H_2O	0.089	0.047	0.138